Kim et al. Int J Concr Struct Mater (2018) 12:73
https://doi.org/10.1186/s40069-018-0296-x

International Journal of Concrete Structures and Materials

RESEARCH Open Access

Tensile Properties of Carbon Fiber-Textile Reinforced Mortar (TRM) Characterized by Different Anchorage Methods

Hee-Seung Kim, Gia Toai Truong, Sung-Ho Park and Kyoung-Kyu Choi*

Abstract

In the present study, tensile tests were carried out to investigate the tensile behaviors of textile reinforced mortar (TRM) composite specimens. The TRM specimens were composed of one layer of carbon fibers, as the reinforcement, and aluminum cement-based mortar, as the matrix. The primary parameter of the test specimens was the anchorage method, which was newly developed to improve the tensile behavior of the composite: spreading the ends of fiber filaments, reinforcing the ends of fiber filaments using glass fiber reinforced polymer tabs or steel rebars, and coating the ends of fiber filaments with aluminum oxide powder. From the test results, it was found that most TRM specimens using developed anchorage methods exhibited ductile behavior. Moreover, the use of the developed anchorage methods could increase the cracking strength and peak strength of the composite specimens up to 66.1 and 97.9%, respectively. The failure mode of the test specimens was governed by a partial rupture of carbon fibers, except for the BASE specimen and specimen reinforced with steel rebars. Finally, the tensile stress–strain relationship of TRM specimens was idealized as bilinear stress–strain response curves following the guidance specified in ACI 549.4R-13.

Keywords: tensile test, carbon fibers, aluminum cement, textile reinforced mortar, anchorage

1 Introduction

Externally bonded composite materials, such as fiber reinforced polymers (FRPs), were widely used as a retrofitting technique by engineers for repairing and strengthening existing masonry and concrete structures. The advantages of FRP composites are; they are lightweight, have corrosion resistance capacity, excellent curing and strength development at room temperature, high tensile strength and elastic modulus, and they can be arranged in various shapes as required in an application (Dai et al. 2011; Ray and Rathore 2015).

However, the cost of organic matrices, such as epoxy resin, is relatively high. The use of organic matrices in FRP composites could result in a reduction of tensile strength at high temperatures, diminish the vapor permeating capacity and low fire resistance. In addition, their compatibility with substrate materials should be carefully considered and there is no reversibility of the installation, such as substitutability and removability (Wu et al. 2014; Cao et al. 2012). Thus, from 1980s, the use of inorganic matrices, e.g. cement-based mortars, as substrates of composite materials, was introduced to expectedly reduce the shortcomings as aforementioned (Brameshuber 2006; Nanni 2012). The development of cement-based mortars resulted in an alternative solution between FRP composites and fiber reinforced mortar (FRM) or textile reinforced mortar (TRM) composites for the structural retrofitting. The TRM composite consisted of fibers in form of textiles and inorganic matrices. The use of textiles as reinforcement fabric could help to overcome the interfacial bonding between fibers and mortar matrix in TRM composites due to their good interlock performance through textile mesh openings (Triantafillou and Papanicolaou 2005; Ombres 2015). However, for the further applications of TRM composites, a number of experimental programs have been performed for better understanding of the mechanical properties, especially tensile behaviors of TRM composites

*Correspondence: kkchoi@ssu.ac.kr
School of Architecture, Soongsil Univ., 369 Sangdo-ro, Dongjak-gu, Seoul, 06978, South Korea
Journal information: ISSN 1976-0485 / eISSN 2234-1315

(Contamine et al. 2011; Donnini et al. 2016; Carozzi et al. 2014; Larrinaga et al. 2014).

Caggegi et al. (2017) investigated experimentally the effects of different reinforcing textile ratios and various kinds of mortar on the tensile behavior of basalt TRM composite specimens. From the test results, it was found that the use of a more resistant mortar resulted in closer cracks in the TRM specimens, which developed at the location of the transversal roving. In addition, using lower strengthening ratio of basalt fibers showed higher tensile strengths. In the study by Donnini and Corinaldesi (2017), the same behavior was also investigated when multiple fabric plies were used in the TRM composites. Moreover, the tensile test results also indicated that the use of coated fabrics, including carbon and basalt fibers, could improve the ultimate tensile strength and modulus of elasticity in the cracked stage (Signorini et al. 2018). The use of cementitious mortar slightly increased the ultimate strength of FRCM composites in comparison to that of lime-based mortar. Besides, in the case of the coated carbon reinforcement fabric, using cementitious mortar instead of a lime-based mortar might change the failure mode from fibers slippage within the matrix to fibers rupture. D'Antino and Papanicolaou (2018) compared the effect of two different tensile test setups including clamping-grip and curved-flange methods on mechanical behavior of inorganic matrix composites. The clamping-grip method was applied to rectangular prism specimens while the curved-flange method was applied to dumbbell specimens. From the test results, it was found that using different test setups resulted in completely different tensile behaviors for the same composite material. Thus, the tensile test results should be consistent with selected test setups. In addition, Donnini and Corinaldesi (2017), De Santis and de Felice (2014), Larrinaga et al. (2013) also investigated that the use of various clamping methods of the TRM specimens at the gripping areas could significantly affect the tensile behaviors of the composite specimens during the direct tensile test.

In this study, experimental studies on the tensile behaviors of TRM specimens were investigated through direct tensile tests according to ACI 549.4R-13 (2013) and AC434 (2011). The specimen was manufactured by using one layer of carbon fiber-textile reinforcement and aluminum cement-based mortar. Different anchorage methods were developed in the gripping areas to improve the tensile behavior of the composite. Such methods included spreading the ends of fiber filaments, reinforcing the ends of fiber filaments using glass fiber reinforced polymer (GFRP) tabs or steel rebars and coating the ends of fiber filaments with aluminum oxide powder. The test results were analyzed in terms of initial stiffness, cracking strength and strain, modulus of elasticity of cracked stage, and peak strength and correlative ultimate strain. Finally, the test results were idealized as bilinear tensile stress–strain response curves based on ACI 549.4R-13 (2013) standard.

2 Experimental Program

2.1 Material Properties

In this study, the textile reinforced mortar (TRM) was fabricated using two primary elements of textile reinforcement and mortar. The textile reinforcement was made from T700S carbon fiber yarns. Each carbon fiber yarn had an average thickness of 0.21 mm and consisted of 24k filaments with filament diameters of 7 μm (see Fig. 1a). In addition, as given by the manufacturer, the tensile strength, elastic modulus and ultimate tensile strain of the carbon fiber filaments were 4900, 230,000 MPa, and 0.015, respectively.

Figure 1b, c present the details of carbon fiber yarn used as a textile reinforcement in this study. It should be noted that such textile reinforcement was fabricated in laboratory by the authors. In general, for each textile reinforcement in the longitudinal direction, four yarns of carbon fiber were used, and the carbon fibers in the longitudinal and horizontal directions were glued together (Fig. 1b). It should also be noted that the longitudinal yarns were composed of three carbon fiber layers and kept straight during the making of the test specimens. Thus, the total thickness of longitudinal yarns was approximately 0.63 mm and the number of carbon fiber filaments was 72,000. The horizontal yarns were composed of two layers of carbon fiber and were in braided shape. Consequently, the horizontal fibers have a theoretical thickness of 0.42 mm and comprised of 42,000 carbon fiber filaments. The textile reinforcement net was intentionally made to be balanced with a spacing of 20 mm, center to center (see Fig. 1c). The free space between yarns was approximately 13.2 mm.

In this study, an alumina cement-based mortar was used as the matrix. Alumina cement has excellent heat resistance and fluidity. In the mortar proportion, granular sand with a granulation ratio of 2.6 was used. The ratio between water and granular sand was 1:2, and that of granular sand and fine aggregate was 1:3. The average compressive strength of mortar was 39.56 MPa, which was tested according to the test standard KS L 5105 (2017).

2.2 Test Specimens

In this study, a direct tensile test of TRM specimens was carried out according to ACI 549.4R-13 (2013) and AC434 (2011). Figure 2 shows the geometrical details of the TRM test specimen. In the figure, the TRM test specimen has a prismatic shape with a rectangular cross

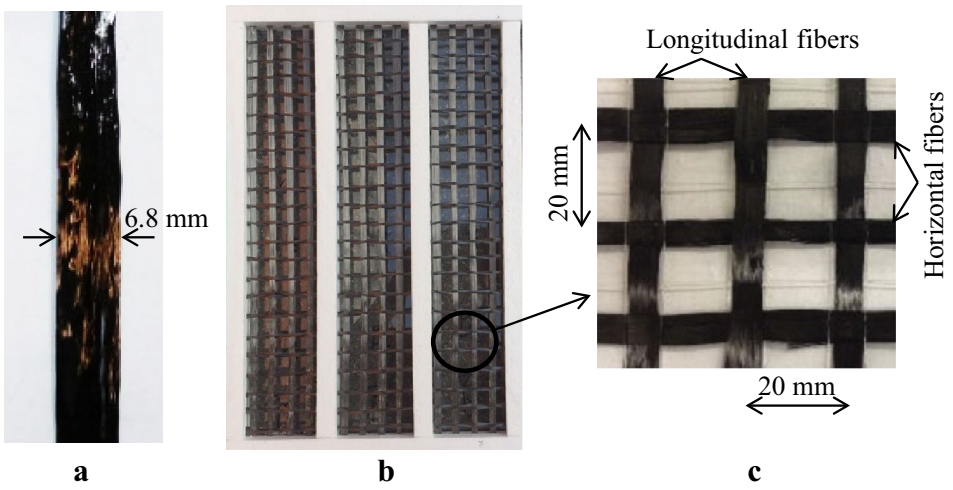

Fig. 1 Details of carbon fiber mesh used as textile reinforcement. **a** Carbon fiber filament provided by manufacturer, **b** Carbon fiber mesh, **c** Geometrical dimensions.

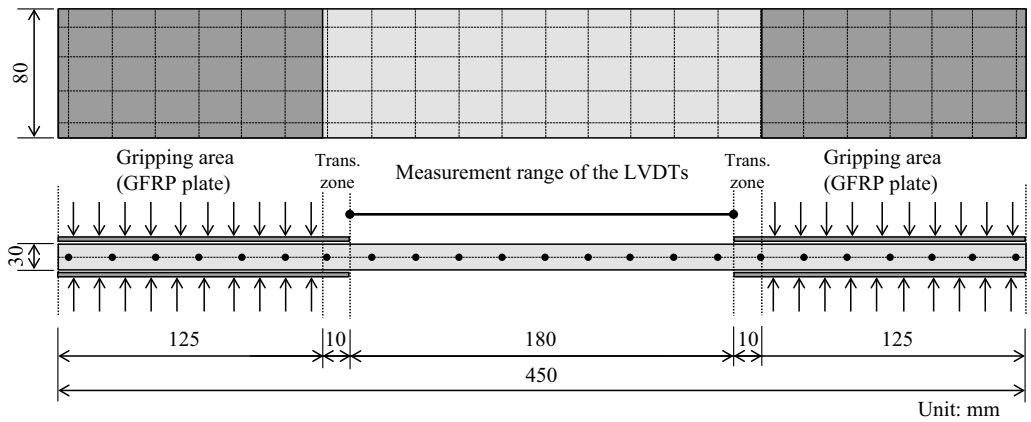

Fig. 2 Typical details of test specimens.

section of 80×30 mm (width $\times$ thickness). The overall length of the TRM test specimen was 450 mm, including the gripping areas, transition zones and a central area in which the strain of the specimen could be measured. The length of the gripping area, transition zone and central area was 125, 10, and 180 mm, respectively. At the gripping areas (at two ends of the test specimen), glass fiber reinforced polymer (GFRP) plates were used as clamping grip materials, and the determination of the gripping length was based on the studies by Donnini and Corinaldesi (2017) and Arboleda et al. (2016). The purpose was to avoid slippage between the test specimen and grip of the testing machine and any damage within the gripping zones. In addition, it was also to induce pressure to the specimen ends to partially enhance the stress-transfer mechanism between the reinforcement fabric and matrix. It was noted that the stress in the transition zone was influenced by the clamping pressure. In some cases the crack had occurred in the transition zone. Therefore, in this study, the GFRP plates in the gripping areas were lengthened to the transition zones to avoid such cracks (see Fig. 2). It also should be noted that all test specimens had the same geometrical properties and clamping grip method. In addition, as shown in Fig. 2, for each test specimen, only one layer of reinforcement fabric was embedded in the mortar matrix.

Five different anchorage methods were developed and experimented in this study. The purpose of the various anchorage methods was to improve the bonding between fibers and matrix to prevent slippage of fibers before reaching the ultimate load-carrying capacity (Carozzi and Poggi 2015; Ascione et al. 2015; Leone et al. 2017).

For each anchorage method, two specimens were made and tested. The number of test specimens was relatively fewer than the other studies (Donnini and Corinaldesi 2017; De Santis and de Felice, 2014; Carozzi et al. 2017; D'Antino and Papanicolaou 2017). Thus, in the further research, for selected anchorage methods, additional test specimens are necessary to improve the test results reliability. The details of anchorage methods are presented in Fig. 3. In the figure, it can be seen that the anchorage was applied only in the gripping areas. It should be noted that to distinguish the TRM test specimens, the specimens were named following the anchorage methods. In Fig. 3a, no anchorage method was applied to the TRM specimen, which was considered as a control specimen and named BASE. Figure 3b describes the details of the TRM specimen named SPREAD. In this test specimen, at the gripping areas, carbon fiber filaments of the textile reinforcement mesh were separated and expanded to enlarge the bonding area between cement mortar and textile reinforcement mesh. In the case of the specimen named TAB (see Fig. 3c), two glass fiber reinforced polymer (GFRP) tabs with dimensions of 60×60 mm were installed inside the specimen to clamp textile reinforcement mesh at the gripping areas. In addition, with holes having a diameter of 5 mm equally arranged on GFRP tabs, it was expected to improve the fixing performance by the pressure between the cement mortar and GFRP tabs. In Fig. 3d, at the end of the specimen named REBAR, two short pieces of D10 reinforcing bars, having diameters of 10 mm and lengths of 80 mm, were wound and fixed by longitudinal carbon fiber filaments of the textile reinforcement mesh. In the case of the specimen named L_COAT (Fig. 3e), carbon fiber filaments of textile reinforcement mesh in the gripping areas were partially impregnated with epoxy resin and coated with aluminum oxide powder that had a diameter of 250 μm (Brauer et al. 1967; Xie and Sherwood 1994). The anchorage details of the specimen named SL_COAT are presented in Fig. 3f. Similar to the L_COAT specimen, carbon fibers in the gripping area of SL_COAT specimen were first impregnated with epoxy resin. Two carbon fiber sheets (60×120 mm) were then attached to clamp such carbon fiber mesh by using epoxy resin. Finally they were also coated with aluminum oxide powder.

2.3 Test Setup and Measurements

Tensile tests were performed using a universal testing machine (UTM) with a loading capacity of 1000 kN. The test setup of the tensile tests for TRM specimens is presented in Fig. 4. As shown in the figure, prior to testing, the gripping areas of the TRM test specimens were clamped with a couple of steel plates and then fastened by use six bolts. The clamping force induced by the fastening force of these six bolts was considered to be the gripping pressure applied to the test specimens. In this study, the clamping force applied to the specimen surface was approximately 126 kN resulted in a clamping stress of 12.6 MPa. This clamping stress was much lower than the compressive strength of the matrix (39.56 MPa), thus the mortar crushing could be avoided. In addition, the slippage between the GFRP and steel plates could also be prevented. The alignment of the test specimen and steel plates was very important to avoid a bending moment that could arise during the loading. The test specimens were then connected with a testing machine through a steel bar, which can rotate freely (see Fig. 4a). Finally, the tests were carried out in a displacement control manner with a test velocity of 0.5 mm/min.

In this study, to measure the tensile strain of the test specimens, two linear variable displacement transformers (LVDT) were installed within the central area (180 mm) along the vertical direction of the test specimens. In addition, another LVDT was centrally placed on the horizontal direction of the test specimen to measure the rotation

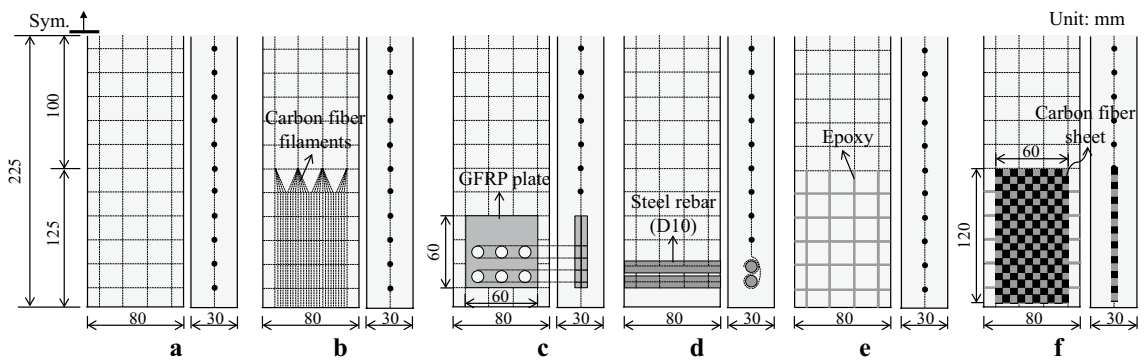

Fig. 3 Details of anchorage methods. **a** BASE, **b** SPREAD, **c** TAB, **d** REBAR, **e** L_COAT, **f** SL_COAT.

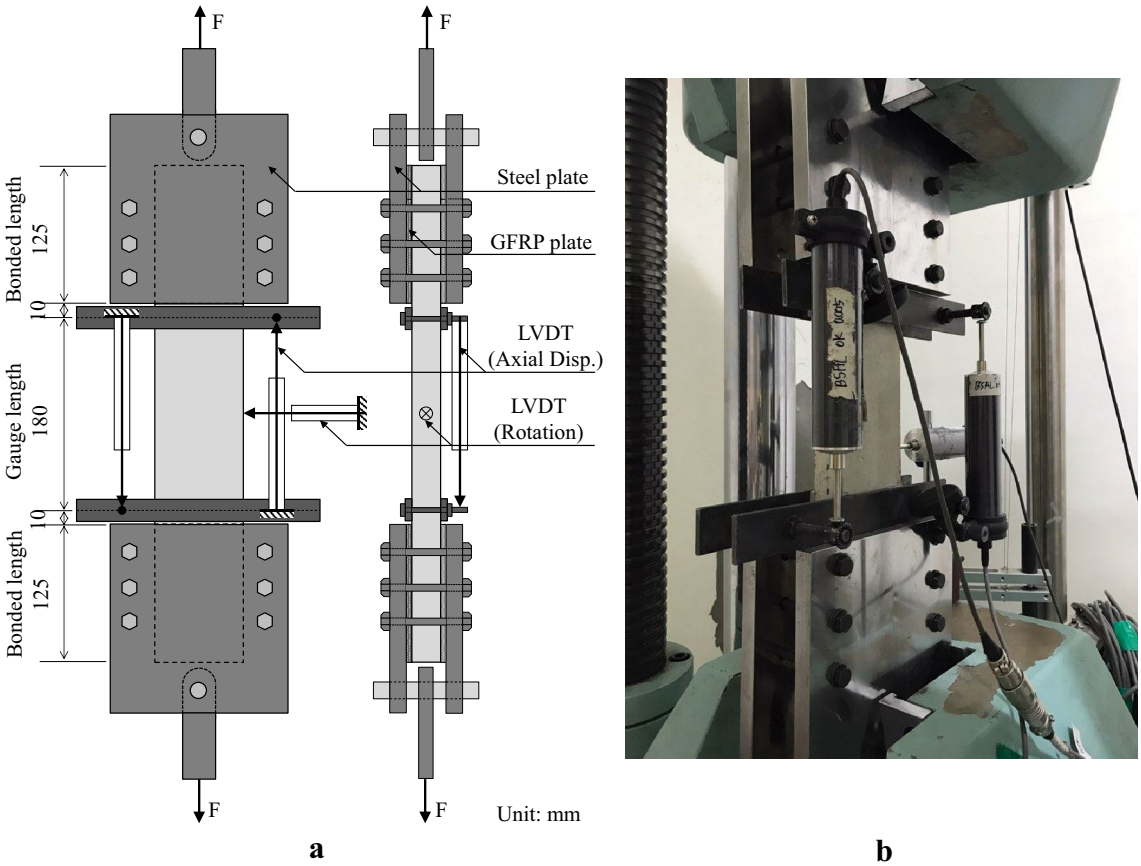

Fig. 4 Tensile test setup. **a** Scheme of test setup, **b** Photo of test setup.

of the specimen due to partial stiffness reduction (see Fig. 4).

3 Experimental Results and Discussions

3.1 Failure Mode

The tensile strength of a TRM test specimen is mainly governed by the strength of carbon fibers and interfacial bonding strength between the carbon fibers and mortar matrix. Figure 5 shows three different types of failure modes that were obtained during tensile test of TRM specimens according to the studies by Loene et al. (2017) and Carozzi et al. (2017). Figure 5a describes the failure mode A, of which tensile failure occurs in the transition zone near the gripping area. This is due to the biaxial stress in the transition zone induced by the combination of compressive force of the gripping clamps and applied tensile force. Failure mode B (Fig. 5b) is caused by rupture of carbon fibers after cracking of the mortar matrix along the length of the test specimen. Meanwhile, in the case of the failure mode C (Fig. 5c), major cracking of the mortar matrix is also observed but the final failure is due to the slippage of carbon fibers within the mortar matrix at the gripping area.

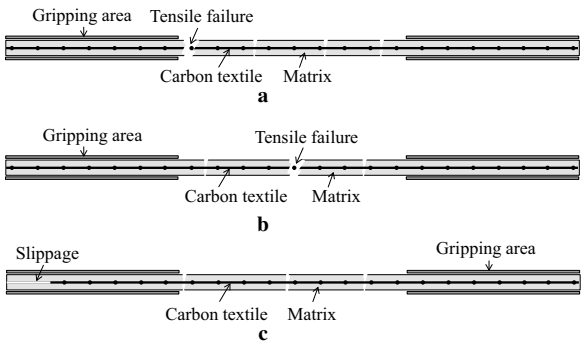

Fig. 5 Failure mode of direct tensile test of TRM test specimens (Leone et al. 2017; Carozzi et al. 2017). **a** Failure mode A, **b** Failure mode B, **c** Failure mode C.

Figure 6 presents crack patterns of the test specimens in this study. In the case of the BASE specimen (Fig. 6a), the cracks occurred near the gripping area. However,

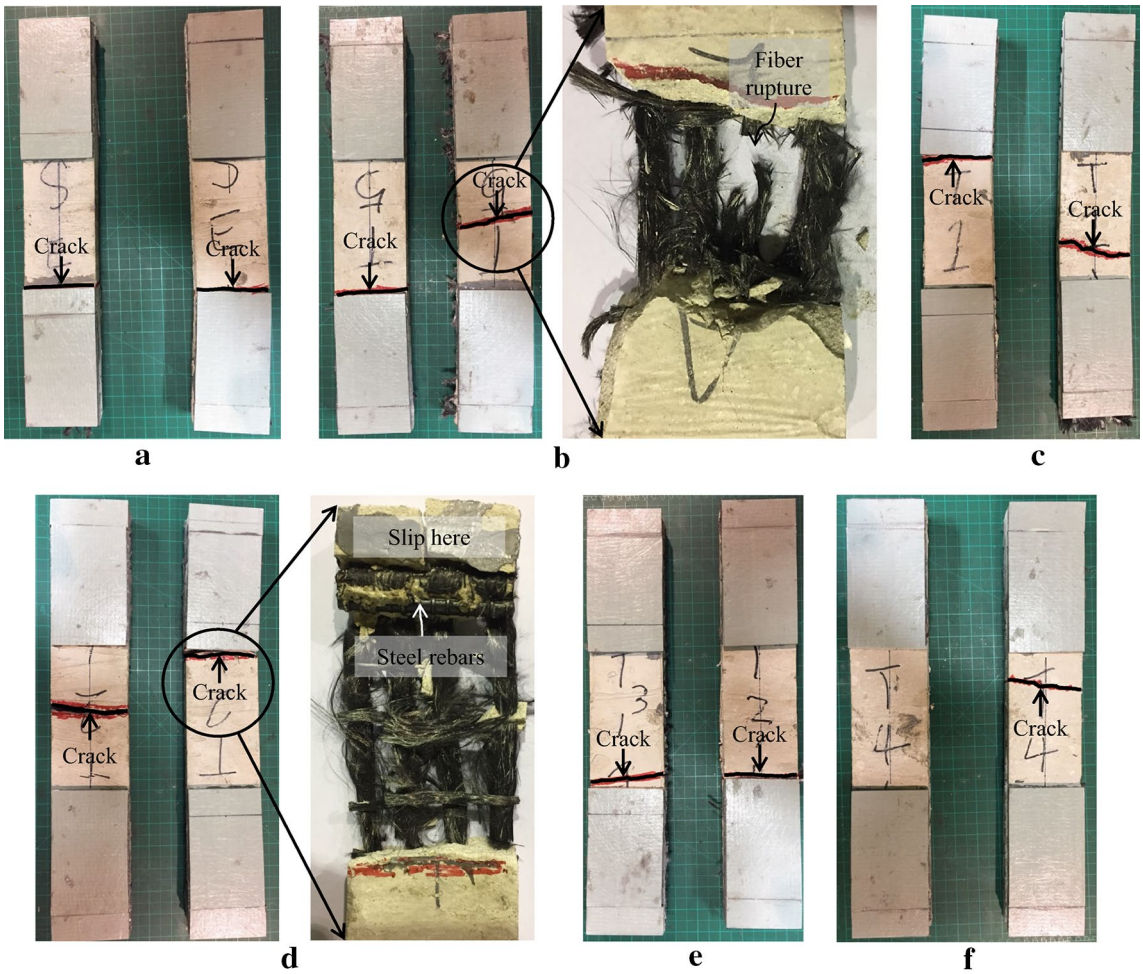

Fig. 6 Failure mode of TRM test specimens in this study. **a** BASE, **b** SPREAD, **c** TAB, **d** REBAR, **e** L_COAT, **f** SL_COAT.

the final failure is due to the fibers slippage within the mortar matrix (failure mode C). The failure mode of the REBAR specimen was also denoted as C, with the subsequent fibers slippage after cracking of the mortar matrix (see Fig. 6d). The slippage between the fibers and mortar could be explained that due to the compressive action of the clamping grip, minor cracks might occur at the interface between the mortar and steel rebars, which could result in the reduction of interfacial bonding in the gripping area. Meanwhile, in the case of the SPREAD specimen, as shown in Fig. 6b, at failure, the longitudinal carbon fibers were ruptured after the first crack of the mortar matrix. However, the failure mode of the SPREAD specimen could be classified into A or B because such cracks occurred both near the gripping area and in the central zone. The other test specimens- including TAB, L_COAT and SL_COAT in Fig. 6c, e, f, respectively-exhibited almost the same failure modes as those of the SPREAD specimen.

3.2 Tensile Behaviors of TRM Test Specimens

In this study, the tensile behaviors of TRM test specimens were investigated in terms of initial stiffness (E) referred to as un-cracked stage of the specimens, cracking strength (f_{ft}), peak strength (f_{fu}) and ultimate strain (ε_{fu}). The initial stiffness was determined in the range of 40% of the cracking strength and correlative strain. The strength was calculated as the applied load divided by the total cross section area of carbon fiber filaments. The ultimate strain was defined as the point from the test results. In the BASE specimen, ε_{fu} was defined in the descending branch. However, in the other specimens, ε_{fu} was defined in the ascending branch. In addition, coefficient of variations of each parameter and envelope of experimental curves was also provided to estimate the variability of the test results.

The stress–strain response curves of the TRM test specimens in this study are presented in Figs. 7, 8 and Table 1. In general, all the test specimens showed a load

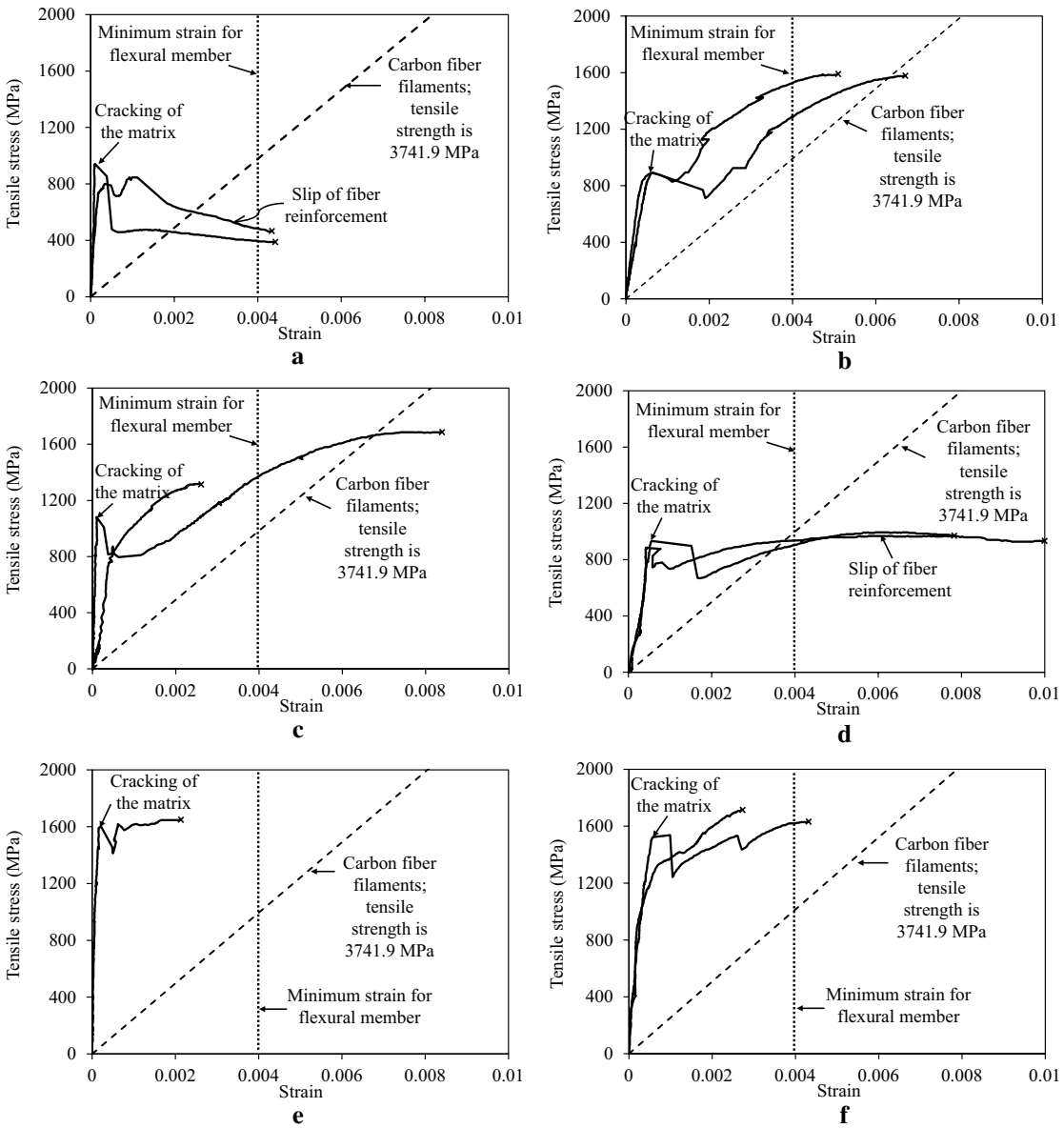

Fig. 7 Stress–strain relationship of test specimens. **a** BASE, **b** SPREAD, **c** TAB, **d** REBAR, **e** L_COAT, **f** SL_COAT.

drop in the experimental curves due to the crack development within the mortar matrix. After that, the final failure of these test specimens was governed by the rupture of carbon fibers or fibers slippage. The contribution of mortar in the uncracked stage is actually apparent because the initial stiffness is considerably higher than that of the carbon fiber filaments. As shown in Fig. 7, the tensile stress–strain curves were located above that of carbon fiber filaments except for the cases of the BASE and REBAR specimens. This is due to the tension stiffening effect of the mortar matrix (D'Antino and Papanicolaou 2017). It should be noted that the ultimate tensile strength and strain of carbon fiber filaments obtained from the test results in this study was 3741.9 MPa and 0.015, respectively.

In the case of the BASE specimen (Fig. 7a), after cracking, residual stress showed a sudden drop due to the slippage of fibers within the mortar matrix. As presented in Table 1, the average initial stiffness of the BASE specimen was 7211.1 GPa with a coefficient of variations (COV) of 0.029. The average cracking strength was 838.8 MPa with a COV of 0.174. In addition, the average ultimate strain was observed as 0.0044 with a COV of 0.016. The peak strength of the BASE specimen could not be determined

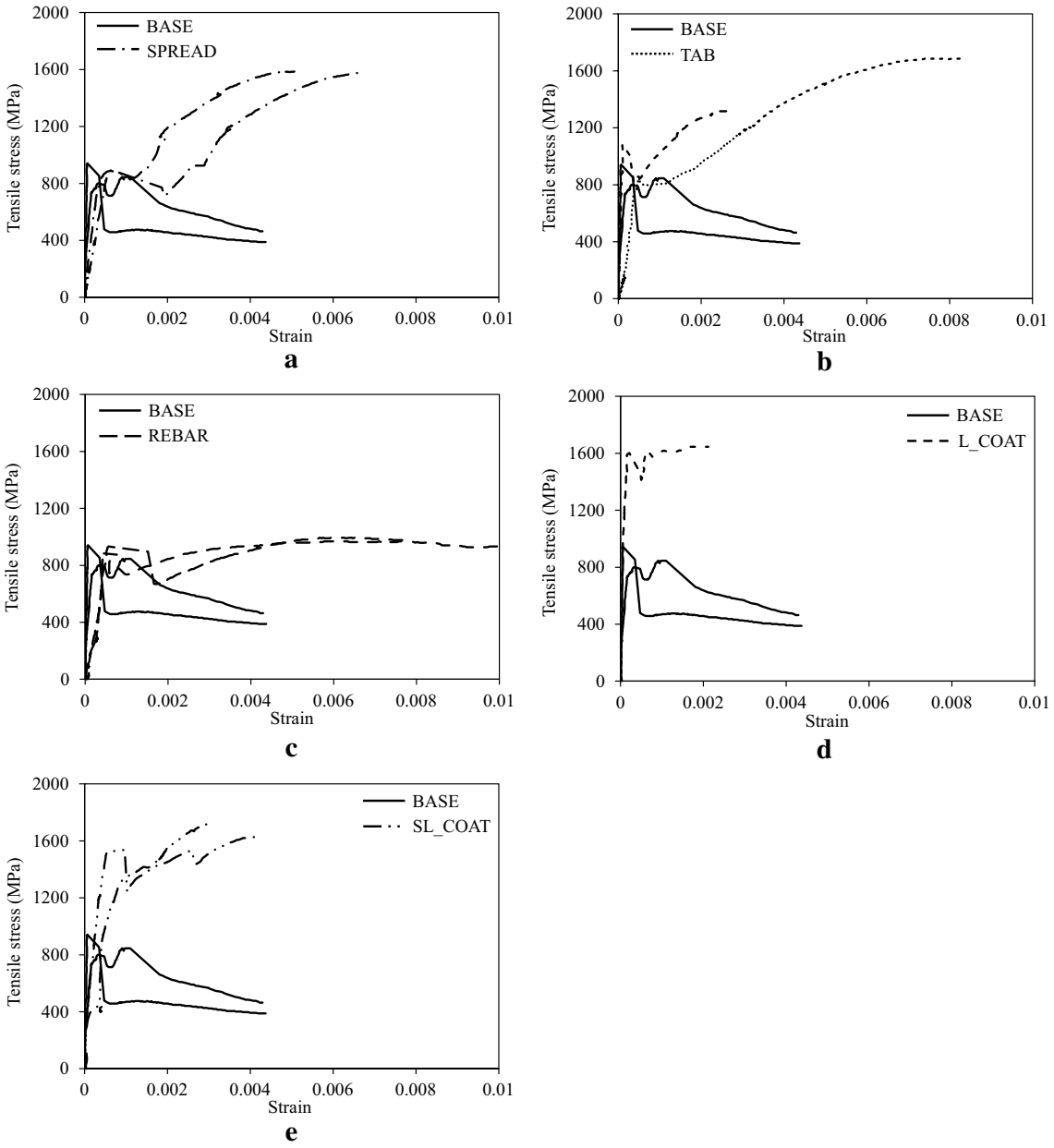

Fig. 8 Effect of anchorage methods on tensile behaviors of test specimens. **a** Effect of SPREAD method, **b** Effect of TAB method, **c** Effect of REBAR method, **d** Effect of L_COAT method, **e** Effect of SL_COAT method

because of the fibers slippage in one specimen. Thus, in this BASE specimen, the peak strength (846.0 MPa) was obtained from only one test specimen. For all that, it can be seen that the peak strength was almost the same as the cracking strength.

Figure 7b presents the stress–strain relationships of the SPREAD specimens. As shown in the figure, during the crack development, the tensile stress was smoothly transferred to the carbon fibers, and the slope of the stress–strain curve was almost parallel to that of the carbon fiber filaments. As presented in Table 1, the initial stiffness, cracking strength, peak strength, and ultimate strain of the SPREAD specimen was 2216.4 GPa, 891.7, 1580.7 MPa and 0.0059. According to ACI 318-14 (2014), for a flexural concrete member, the minimum tensile strain that is required is 0.004. Thus, the obtained ultimate strain is greater than that specified in the ACI 318-14 (2014). From Fig. 7b and Table 1, it can be seen

Table 1 Tensile test results of TRM specimens in this study.

Specimen	Initial stiffness		Cracking strength		Cracking strain		Elastic modulus of cracked stage		Peak strength		Ultimate strain		f_{fu}/f_{ft}	Failure mode
	E (GPa)	COV	f_{ft} (MPa)	COV	ε_{ft}	COV	E_f (GPa)	COV	f_{fu} (MPa)	COV	ε_{fu}	COV		
BASE	7211.1	0.029	838.8	0.174	0.00012	0.184	39.2[a]	–	846.0[a]	–	0.0044	0.016	1.01	C
SPREAD	2216.4	0.045	891.7	0.0035	0.00040	0.054	155.3	0.329	1580.7	0.0039	0.0059	0.192	1.77	A or B
TAB	7451.4	1.051	976.7	0.153	0.00027	0.987	106.4	0.469	1501.1	0.173	0.0055	0.740	1.54	A or B
REBAR	1545.6	0.037	864.3	0.104	0.00059	0.072	8.6	1.003	987.6	0.0281	0.01	0	1.14	C
L_COAT	10596.2[a]	–	1602.5[a]	–	0.00015[a]	–	19.1[a]	–	1646.0[a]	–	0.0021[a]	–	1.02	A or B
SL_COAT	3609.3	0.080	1393.2	0.118	0.00039	0.018	120.5	0.912	1673.9	0.035	0.0035	0.323	1.20	A or B

[a] Test results obtained from only one test specimen.

that the ultimate strain of the two SPREAD specimens showed a scatter with a COV of 0.192. Meanwhile, the initial stiffness, cracking strength and peak strength of the two SPREAD specimens were almost the same. Figure 8a compared the tensile behaviors of the SPREAD specimen with those of the BASE specimen. It is clear that by using a spread anchorage method, the cracking strength increased approximately 6.3%. In particular, the peak strength increased significantly up to 86.8%. It was attributed to the fact that the spread of carbon fibers in the gripping areas increased the interfacial bonding area between fibers and mortar matrix, and thus caused a considerable improvement of the bonding strength of the fibers and matrix.

The stress–strain response curves and mechanical parameters of the TAB specimen are presented in Fig. 7c and Table 1, respectively. In terms of the first crack, the average cracking strength was 976.7 MPa with a COV of 0.153. The average peak strength and ultimate strain was 1501.1 MPa and 0.0055, respectively. The ultimate strain was also higher than the required value (0.004) specified in ACI 318-14 (2014). Clearly, similar to the SPREAD specimen, the use of GFRP tabs as an anchorage method could significantly increase both the cracking and peak strengths. Figure 8b shows the comparison of test results of the TAB specimen with those of the BASE specimen. The increase of the TAB specimen in terms of the cracking and peak strengths compared to those of the BASE specimen were approximately 16.4 and 77.4%, respectively. The initial stiffness of the TAB specimen was also higher than that of the BASE specimen. However, it showed a significant scatter (COV = 1.051).

Figure 7d shows the stress–strain response curves of the REBAR specimen. As shown in the figure, the response curves of the REBAR specimen were similar to those of the BASE specimen. However, in comparison to the BASE specimen, the residual stress after cracking of the REBAR specimen was significantly greater, and showed almost a flat trend until failure of the test specimen. The REBAR specimen showed ductile behavior with the ultimate strain up to 0.01.

Figure 7e presents the stress–strain curve obtained from the test results of the L_COAT specimen. It should be noted that one of the L_COAT test specimens failed during manufacturing. Thus, the test parameters were obtained from only one specimen. The cracking and peak strengths of the L_COAT specimen were 1602.5 and 1646.0 MPa, respectively. It is evident that the cracking and peak strengths of the L_COAT specimen were greater than those of the BASE specimen (see Fig. 8d and Table 1). In addition, the initial stiffness of the L_COAT specimen also increased up to 46.9%. Meanwhile, the ultimate strain of the L_COAT specimen showed relatively low with a value of 0.0021, which was considerably less than the minimum requirement of the flexural strain of 0.004 (ACI 318-14 2014).

The experimental results of TRM specimens, using SL_COAT as an anchorage method, are presented in Fig. 7f in terms of stress–strain response curves. The mechanical parameters are presented in Table 1. From Fig. 7f and Table 1, the average cracking and peak strengths of the SL_COAT specimen were 1393.2 and 1673.9 MPa, respectively (see Table 1). Figure 8e presents the comparison between the SL_COAT and BASE specimens in terms of stress–strain behavior. Similar to the L_COAT specimen, the use of a combination of carbon fiber sheets and coating carbon fiber filaments, with epoxy and aluminum oxide powder, could significantly increase the cracking and peak strengths of the SL_COAT specimen up to 66.1 and 97.9%, respectively, compared to those of the BASE specimen. Meanwhile, the obtained ultimate strain was in a range of 0.0026–0.0043. In general, the SL_COAT specimen showed a brittle failure with an average ultimate strain of 0.0035, which was less than

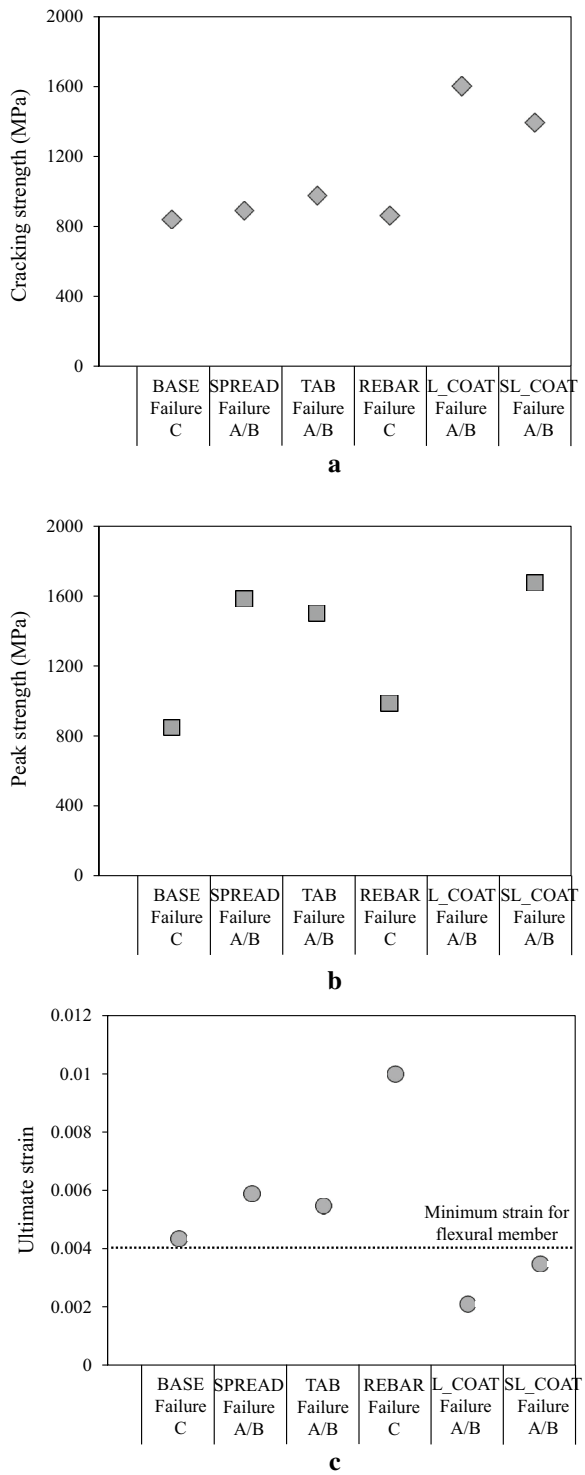

Fig. 9 Comparison of average cracking strength, average peak strength and average ultimate strain of TRM test specimens. **a** Effect of anchorage methods on cracking strength, **b** Effect of anchorage methods on peak strength, **c** Effect of anchorage methods on ultimate strain.

the flexural strain (0.004) specified in ACI 318-14 (2014). Moreover, the initial stiffness was also less than that of the BASE specimen, approximately 49.9%.

From the obtained test results in this study, it could be found that the most developed anchorage methods showed effectiveness on improving the mechanical behaviors of the TRM specimens. Figure 9 presents the comparison of the test results obtained from different anchorage methods in terms of the cracking and peak strengths, and ultimate strain. As shown in Fig. 9a, b, the coated specimens with aluminum oxide powder (L_COAT and SL_COAT) showed effectiveness in the increase of cracking strength. In addition, except for the specimen reinforced with steel rebar (REBAR), the remained anchorage methods showed effectiveness in the increase of the peak strength. In Fig. 9c, the coated specimens showed less ultimate strains compared to the other cases. In Table 1, the ratio (f_{fu}/f_{ft}) between the peak strength and cracking strength was presented. As shown in the table, the SPREAD and TAB specimens showed high values of f_{fu}/f_{ft}; 1.77 for SPREAD and 1.54 for TAB specimens, respectively. This means that the peak strength was significantly higher than the cracking strength.

3.3 Idealized Stress–Strain Response Curves of TRM Test Specimens

In this study, idealized tensile stress–strain response curves of the TRM test specimens were proposed based on the guidance specified in the test standard ACI 549.4R-13 (2013). The response curves were simply plotted as bilinear curves with only one transition point (cracking point) between the cracked and uncracked stages. Figure 10 illustrates a bilinear stress–strain curve

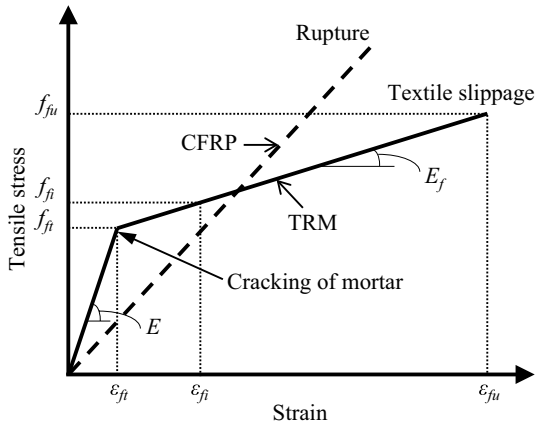

Fig. 10 Idealized stress–strain curve of TRM test specimen according to ACI 549.4R-13 (2013).

of a TRM test specimen. In the figure, it can be seen that in the uncracked stage, the stress–strain curve is linearly characterized by the initial stiffness (E); whereas in the cracked stage, the stress–strain curve is linearly characterized by the modulus of elasticity E_f. The elastic modulus of cracked stage can be calculated as shown in Eq. (1) below;

$$E_f = \Delta f / \Delta \varepsilon = \left(0.9 f_{fu} - 0.6 f_{fu}\right) \Big/ \left(\varepsilon_{0.9 f_{fu}} - \varepsilon_{0.6 f_{fu}}\right). \quad (1)$$

Moreover, as shown in Fig. 10, to characterize the tensile behavior of a TRM specimen, additional mechanical parameters should be considered, including peak strength (f_{fu}), correlative ultimate strain (ε_{fu}), tensile strength (f_{ft}) and correlative strain (ε_{ft}) at the transition point. From the experimental results, such mechanical parameters could be determined and the obtained values are presented in Table 1.

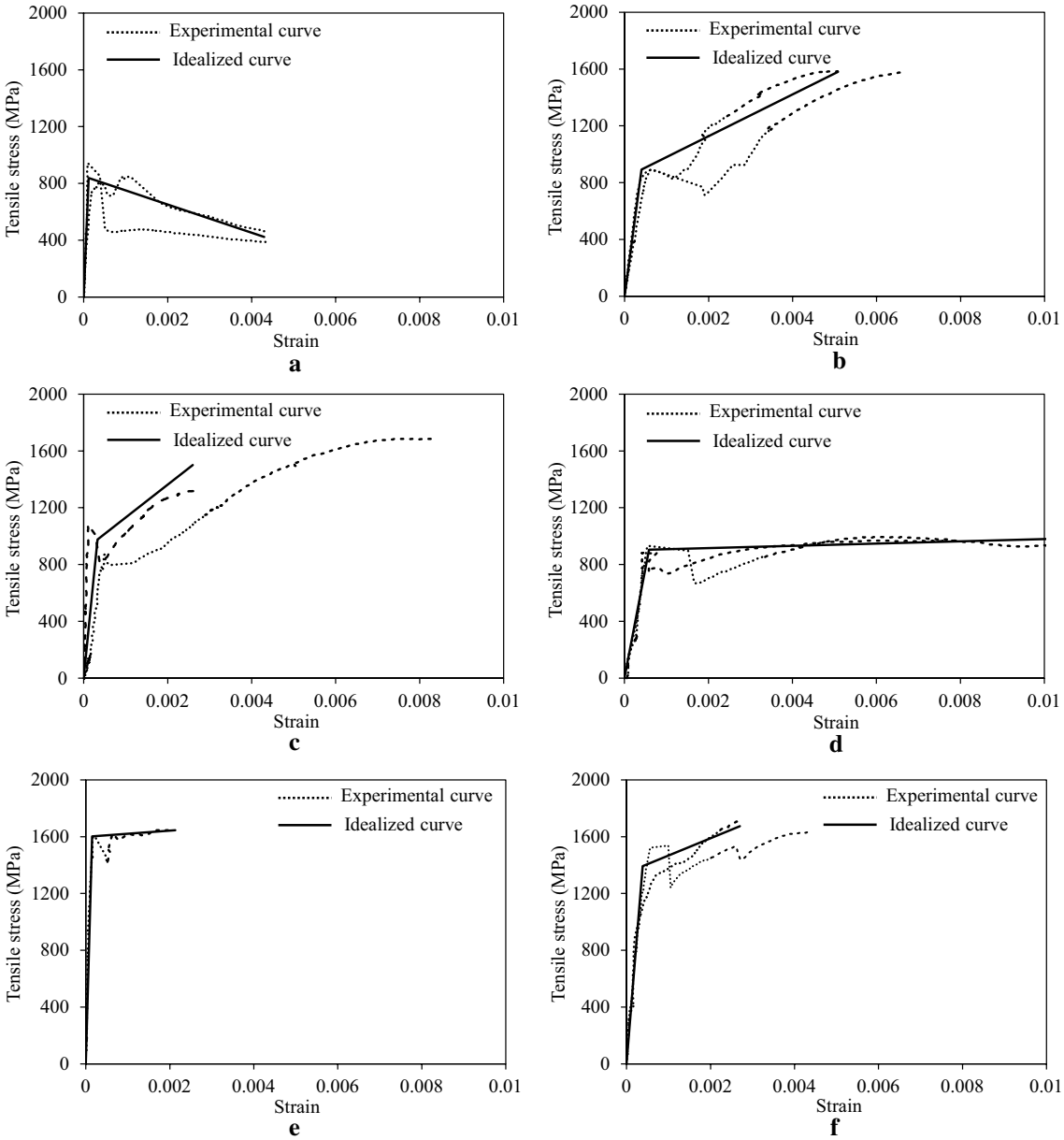

Fig. 11 Idealized and experimental stress–strain curves of TRM test specimens in this study. **a** BASE, **b** SPREAD, **c** TAB, **d** REBAR, **e** L_COAT, **f** SL_COAT.

Figure 11 presents the idealized tensile stress–strain response curves of the TRM test specimens in this study. In general, the method proposed by ACI 549.4R-13 (2013) could be effectively applied to illustrate the stress–strain curve of TRM specimens using different anchorage methods. In particular, in the first stage (uncracked stage), the analytical stress–strain curves showed a good agreement with the experimental curves. In the second stage (crack stage), in the cases of specimens SPREAD (Fig. 11b), TAB (Fig. 11c), and SL_COAT (Fig. 11f), the analytical stress–strain curves were slightly above the experimental results. It was due to the fact that the elastic modulus of cracked stage (E_f) was slightly higher than that obtained from the experimental results. Note that E_f was calculated based on the mechanical parameters including peak strength (f_{fu}) and correlative ultimate strain (ε_{fu}) [see Eq. (1)], which might be affected by the anchorage methods used in this study. However, the number of test data was very limited in this study. Thus, to get improved E_f, accumulated test results are needed considering the anchorage effect.

4 Conclusions

Tensile tests have been performed to investigate the tensile behaviors of TRM specimens, which were made from carbon fiber-textile reinforcement and aluminum cement-based mortar. Five different anchorage methods in the gripping areas- including SPREAD, TAB, REBAR, L_COAT and SL_COAT- were proposed to enhance the mechanical properties of TRM specimens. The primary findings are as follows:

1. Most failure mode of test specimens was governed by partial fibers rupture after cracking occurred in the mortar. However, the REBAR specimen was governed by fibers slippage within the mortar matrix.
2. Due to the tension stiffening effect of mortar matrix, except for the case of REBAR specimen, the tensile stress–strain response curves of other test specimens were located above that of carbon fiber filaments.
3. The cracking and peak strengths of the TRM specimens, using anchorage methods, increased significantly up to 66.1 and 97.9%, respectively, compared to those of the BASE specimen.
4. The use of SPREAD and TAB methods showed a ductile behavior with the ultimate strain up to 0.0059 and 0.0055, respectively. The REBAR specimen also exhibited a greatly ductile behavior with an ultimate strain of up to 0.01. Meanwhile, the use of coating and carbon fiber sheets as anchorage methods resulted in brittle behaviors of the L_COAT and SL_COAT specimens with ultimate strains lower than the minimum strain for the flexural member (0.004), as specified in ACI 318-14.
5. The tensile stress–strain behavior of the TRM specimens in this study could be simply idealized by bilinear stress–strain response curves based on the test standard ACI 549.4R-13. The mechanical parameters for the idealized bilinear stress–strain curves were obtained from the test results.

Authors' contributions

All of the authors contributed critically to the conception, experiment, analyzing the test data as well as drafting and revision of the manuscript. All authors read and approved the final manuscript.

Acknowledgements

This research was supported by a Grant (18CTAP-C130221-02) from Infrastructure and Transportation Technology Promotion Research Program funded by Ministry of Land, Infrastructure and Transport of Korean Government.

Competing interests

The authors declare that they have no competing interests.

Availability of data and materials

The data and materials have been experimentally performed and investigated by the authors.

Consent for publication

Accepted.

Ethics approval and consent to participate

Not applicable.

Funding

Accepted with article-processing charge (APC) policies.

Publisher's Note

Received: 8 March 2018 Accepted: 4 July 2018
Published online: 27 November 2018

References

AC434. Acceptance criteria for masonry and concrete strengthening using fiber-reinforced cementitious matrix (FRCM) composite systems. A Subsidiary of the International Code Council, Birmingham, UK; 2011.

ACI 318-14. (2014). *Building code requirements for structure concrete (ACI 318-14)*. Farmington Hills: American Concrete Institute.

ACI 549.4R-13. (2013). *Guide to design and construction of externally bonded fabric-reinforced cementitious matrix (FRCM) systems for repair and strengthening concrete and masonry structures*. Farmington Hills: American Concrete Institute.

Arboleda, D., Carozzi, F. G., Nanni, A., & Poggi, C. (2016). Testing procedures for the uniaxial tensile characterization of fabric-reinforced cementitious matrix composites. *Journal of Composites for Construction, 20*(3), 1–11.

Ascione, L., de Felice, G., & De Santis, S. (2015). A qualification method for externally bonded fibre reinforced cementitious matrix (FRCM) strengthening systems. *Composites: Part B, 78,* 497–506.

Brameshuber, W. (2006) *State-of-the-art report of RILEM Technical Committee 201-TRC: Textile reinforced concrete*. RILEM Report 36.

Brauer, G. M., McLaughlin, R. P., Huget, E. F. (1967) *Aluminum oxide as a reinforcing agent for zinc oxide-eugenol-eba cements*. National Bureau of Standards Report.

Caggegi, C., Laoye, E., Djama, K., Bassil, A., & Gabor, A. (2017). Tensile behaviour of a basalt TRM strengthening system: Influence of mortar and reinforcing textile ratios. *Composites: Part B, 130,* 90–102.

Cao, S., Wu, Z., & Li, F. (2012). Effects of temperature on tensile strength of carbon fiber and carbon/epoxy composite sheets. *Advanced Materials Research, 476–478,* 778–784.

Carozzi, F. G., Bellini, A., D'Antino, T., de Felice, G., Focacci, F., Hojdys, L., et al. (2017). Experimental investigation of tensile and bond properties of carbon-FRCM composites for strengthening masonry elements. *Composites: Part B, 128,* 100–119.

Carozzi, F. G., Milani, G., & Poggi, C. (2014). Mechanical properties and numerical modeling of fabric reinforced cementitious matrix (FRCM) systems for strengthening of masonry structures. *Composite Structures, 107,* 711–725.

Carozzi, F. G., & Poggi, C. (2015). Mechanical properties and debonding strength of fabric reinforced cementitious matrix (FRCM) systems for masonry strengthening. *Composites: Part B, 70,* 215–230.

Contamine, R., Si Larbi, A., & Hamelin, P. (2011). Contribution to direct tensile testing of textile reinforced concrete (TRC) composites. *Materials Science and Engineering A, 528,* 8589–8598.

D'Antino, T., & Papanicolaou, C. (2017). Mechanical characterization of textile reinforced inorganic-matrix composites. *Composites: Part B, 127,* 78–91.

D'Antino, T., & Papanicolaou, C. (2018). Comparison between different tensile test set-ups for the mechanical characterization of inorganic-matrix composites. *Construction and Building Materials, 171,* 140–151.

Dai, J.-G., Bai, Y.-L., & Teng, J. G. (2011). Behavior and modeling of concrete confined with FRP composites of large deformability. *Journal of Composites for Construction, 15*(6), 963–973.

De Santis, S., & de Felice, G. (2014). Tensile behavior of mortar-based composites for externally bonded reinforcement systems. *Composites: Part B, 68,* 401–413.

Donnini, J., & Corinaldesi, V. (2017). Mechanical characterization of different FRCM systems for structural reinforcement. *Construction and Building Materials, 145,* 565–575.

Donnini, J., Corinaldesi, V., & Nanni, A. (2016). Mechanical properties of FRCM using carbon fabrics with different coating treatments. *Composites: Part B, 88,* 220–228.

KS L 5105. (2017). *Testing method for compressive strength of hydraulic cement mortars*. Seoul: Korean Standard Association.

Larrinaga, P., Chastre, C., Biscaia, H. C., & San-Jose, J. T. (2014). Experimental and numerical modeling of basalt textile reinforced mortar behavior under tensile stress. *Materials and Design, 55,* 66–74.

Larrinaga, P., Chastre, C., San-Jose, J. T., & Garmendia, L. (2013). Non-linear analytical model of composites based on basalt textile reinforced mortar under uniaxial tension. *Composites Part B Engineering, 55,* 518–527.

Leone, M., Aiello, M. A., Balsamo, A., Carozzi, F. G., Ceroni, F., Corradi, M., et al. (2017). Glass fabric reinforced cementitious matrix: Tensile properties and bond performance on masonry substrate. *Composites: Part B, 127,* 196–214.

Nanni, A. (2012). A new tool in the concrete and masonry repair toolbox: Strengthening with fiber-reinforced cementitious matrix composites. *Concrete International, 34*(4), 43–49.

Ombres, L. (2015). Analysis of the bond between fabric reinforced cementitious mortar (FRCM) strengthening systems and concrete. *Composites: Part B, 69,* 418–426.

Ray, B. C., & Rathore, D. (2015). A review on mechanical behavior of FRP composites at different loading speeds. *Critical Review in Solid State and Materials Science, 40*(2), 119–135.

Signorini, C., Nobili, A., Gonzalez, E. I. C., & Siligardi, C. (2018). Silica coating for interphase bond enhancement of carbon and AR-glass textile reinforced mortar (TRM). *Composites: Part B, 141,* 191–202.

Triantafillou, T. C., & Papanicolaou, C. G. (2005). Textile reinforced mortars (TRM) versus fiber reinforced polymers (FRP) as strengthening materials of concrete structures. *International Concrete Abstracts Portal: Special Publication, 230,* 99–118.

Wu, Z., Wang, X., Zhao, X., & Noori, M. (2014). State-of-the-art review of FRP composites for major constructions with high performance and longevity. *International Journal of Sustainable Materials and Structural Systems, 1*(3), 201–231.

Xie, Y., & Sherwood, P. M. A. (1994). Coatings of aluminum oxide and magnesium oxide on carbon fiber surfaces. *Chemistry of Materials, 6*(5), 650–657.